Plasmon Resonances of Highly Doped Two-Dimensional MoS_2

Yichao Wang[1], Jian Zhen Ou[1], Adam F. Chrimes[1], Benjamin J. Carey[1], Torben Daeneke[1], Manal M Y A Alsaif[1], Majid M. Mortazavi[2], Serge Zhuiykov[3], Nikhil Medhekar[2], Madhu Bhaskaran[1], James R. Friend[4], Michael S. Strano[5] & Kourosh Kalantar-zadeh[1]

[1] School of Electrical and Computer Engineering, RMIT University, Melbourne, Victoria, Australia

[2] Department of Materials Engineering, Monash University, Clayton, Victoria, Australia

[3] Division of Materials Sciences and Engineering, CSIRO, Highett, Victoria, Australia

[4] Department of Mechanical and Aerospace Engineering, Jacobs School of Engineering, University of California, San Diego CA USA

[5] Department of Chemical Engineering, Massachusetts Institute of Technology, Cambridge MA USA

Table of Contents Graphic

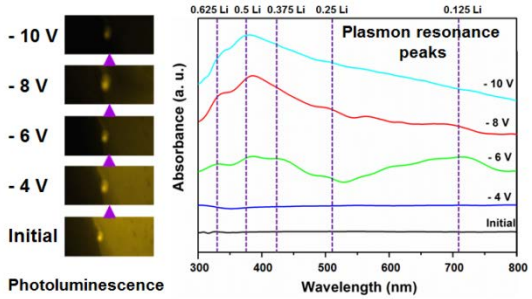

ABSTRACT: The exhibition of plasmon resonances in two-dimensional (2D) semiconductor compounds is desirable for many applications**.** Here, by electrochemically intercalating lithium into 2D molybdenum disulphide (MoS_2) nanoflakes, plasmon resonances in the visible and near UV wavelength ranges are achieved. These plasmon resonances are controlled by the high doping level of the nanoflakes after the intercalation, producing two distinct resonance peak areas based on the crystal arrangements. The system is also benchmarked for biosensing using bovine serum albumin. This work provides a foundation for developing future 2D MoS_2 based biological and optical units.

KEYWORDS: Two-dimensional; MoS_2; Plasmonics; Doping; Electrochemical intercalation; Biosensor

To create practical nanophotonic devices at low dimensions, electromagnetic energy need to be confined and controlled well below the diffraction limits, the light waves should propagate at relatively low losses and the devices should favorably operate at commercial wavelengths. [1, 2] Plasmon resonances in conventional metallic systems (*e.g.* gold and silver) can be described using collective electron oscillations excited by external light.[3] They lead to strong confinements of electric fields near the surface of metallic materials, stimulating various surface effects such as enhanced absorption and Raman signal enhancement. However, due to the nature of the electronic structures in metals and that their free carrier concentrations cannot be readily controlled by various stimuli, tuneability of plasmon resonances is challenging for switching or modulation applications.[3, 4]

A material with a purely real and negative permittivity ($\varepsilon'' = 0$ and $\varepsilon' < 0$) in all wavelengths would be an ideal plasmonic candidate, which is theoretically impossible to create due to the causality condition.[3] One approach to achieve materials to at least satisfy the plasmon condition within selected wavelength ranges is to heavily dope semiconductors, creating enough free charge carriers to render them quasi-metallic.[5] It has been shown that doping of a selected semiconductors, such as Si, SeGe, GaAs, GaN, ZnO and indium tin oxide (ITO), can increase their carrier concentrations and tune them.[3] By doping, metal-like optical properties ($\varepsilon' < 0$) are achieved in the spectrum of interest. Drude equation sets a minimum limit for the carrier concentration that should be met before seeing plasmonic properties.[3] This is generally larger than 10^{21} cm^{-3} value for observing plasmonic peaks in the NIR and visible regions.

Recently, plasmonics of two dimensional (2D) materials have attracted significant attention due to their desirable dispersion relation.[6] According to the 2D dispersion equation, the cut-off frequency limit is eliminated.[3] Additionally their large tuneability, high doping

(ultra-doping) range and the existence of favorable depolarization factors allow for their better control. Amongst 2D transition metal dichalcognides, molybdenum disulfide (MoS_2) has recently received increased attention.[7-10] The demonstration of relatively large free charge carrier mobilities and revealing a direct bandgap in single layer MoS_2 have been especially exciting discoveries in recent years.[11-14] Challenges remain regarding the generation of plasmons in intrinsic 2D MoS_2, which accommodates massive electrons (unlike graphene) and relatively low carrier concentrations (10^{12} to 10^{14} cm^{-3}).[6] Consequently, it has been theoretically shown that intrinsic 2D MoS_2 plasmon resonances only appear at relatively low frequencies, in the far infrared and terahertz regimes.[6] Hence, doping is crucial to increase the carrier concentration in order to obtain plasmon resonances at commercially useful wavelengths. Additionally, the demonstration of plasmon harvested energy at such wavelengths can be potentially used for *in vivo* therapeutic applications and catalysis.[15]

The most commonly encountered polymorph of intrinsic MoS_2 in 2D format is 2H with trigonal prismatic coordination. 2H MoS_2 has two S–Mo–S units in the unit cell and shows a semiconducting behavior due to its atomic arrangement. In 1T metastable phase, which is metallic with high free carrier concentration, Mo atoms are coordinated octahedrally by the sulfur atoms in one unit cell. It is known that this 2H semiconducting phase can be reversibly transformed into 1T metallic phase *via* an intra-layer atomic glide.[16] This involves a transversal displacement of one of the S planes. Intercalation of Li is an effective method for inducing such a conversion that accompanies a charge transfer from Li to MoS_2,[17] increasing the free carrier concentrations to desired levels. A local rearrangement of atomic structure from 2H to 1T occurs to accommodate the intercalated species.[18]

In this study, we explore plasmon resonances of ultra-doped 2D MoS_2 nanoflakes in the visible and near UV ranges. This ultra-doping is achieved using electrochemical means *via* lithium intercalation. A set of tests are presented to evidence the presence of plasmon,

including the electron energy loss spectroscopy and resonance peak shifts in the media of different dielectric constants.

The 2D MoS_2 nanoflakes suspended in an *N*-methylpyrrolidinone (NMP) solution are prepared from MoS_2 bulk powder using a grinding-assist liquid phase exfoliation technique[8, 19, 20] (see the Methods Section for details). The process results in 2D flakes with lateral dimensions mainly of 10 to 80 nm and thicknesses corresponding to 2 to 7 monolayers (statistical analysis from a large number of atomic force microscopy (AFM) measurements is presented in Table S1). The transition from MoS_2 to Li_xMoS_2 through an intercalation process is carried out by applying different voltages using a Li^+ containing electrolyte. AFM imaging confirms the presence of planar 2D structures made of multiple fundamental layers both before and after the intercalation process (examples in Figures 1a and b). High-resolution transmission electron microscopy (HRTEM - Figure 1c) shows that the initial 2D MoS_2 nanoflakes have a fringe spacing of 0.27 nm, corresponding to the (100) lattice plane.[8] The selected area electron diffraction (SAED) pattern of this flake is indexed to the near perfect planar 2H MoS_2. Some of the structures are found to show disordered polycrystalline features after lithium intercalation, which can be seen from the polycrystalline 'ring' SAED pattern (Figure 1d). The intercalation of the Li^+ ions into the crystal lattice expands the crystal structure[8] and eventually produces cracked crystals possessing smaller domains.[21, 22] X-ray diffraction (XRD) is used for further estimation of the onset of cracking (Figure S1 and Supporting Information Section S2).

The evolution of the lithium intercalation by electrochemical means is evident from Raman spectroscopy. From Figure 1e, two distinct Raman peaks are found at 383 and 406 cm^{-1} for the pristine 2D MoS_2 nanoflakes, corresponding to basal plane (E^1_{2g}) and vertical plane (A_{1g}) vibrations of Mo–S bonds in 2H MoS_2,[23-25] respectively. For intercalation at –4 V, the

spectrum is nearly the same as the pristine flakes. For an applied voltage below –6 V, Raman shifts for both E^1_{2g} and A_{1g} modes are observed and the gap between these two modes, in terms of the wavenumber, is increased. The peak shift in the Raman spectra is due to additional strain in the lattice suppressing the vibration of Mo–S bonds after the lithium intercalation.[23] When voltages below –6 V are applied, as an increasing amount of Li^+ at larger energies are intercalated into the 2D MoS_2 planes, more electrons are transferred to the MoS_2 electronic orbitals, leading to a 2H to 1T phase transition and formation of Li_xMoS_2 compounds.[26]

A phase transition from 2H to 1T is also found using X-ray photoelectron spectroscopy (XPS) measurements at low applied voltages (surface of the films was etched for 60 s before the pattern acquisition). From Figure 1f, for the pristine MoS_2 and Li^+ intercalated MoS_2 at an applied voltage of –4 V, $Mo3d_{3/2}$ and $Mo3d_{5/2}$ peaks can be observed at 232.6 and 229.4 eV, respectively, indicating that the elemental Mo keeps the +4 oxidation state and the 2D crystal structures remain dominant in the 2H phase.[8, 27] When the applied voltage is decreased to –6 V, shoulders appear at 231.2 and 227.9 eV. Deconvolution of the curve reveals that these are weak peaks corresponding to the 1T phase of MoS_2, indicating the structure of MoS_2 begins a phase transition from 2H to 1T. The lower binding energy of the new peaks confirms the intercalation of the Li species in the 2D MoS_2, leading to a lower oxidation state of Mo.[28] Deconvolution of the curve corresponding to an applied voltage of less than –8 V reveals the strong intensity of the emerging peaks with downshifted binding energies, stronger than even the –6 V case, suggesting that a greater portion of the 2D MoS_2 flakes undergoes a phase transition to the 1T phase.[17, 29]

The intercalation of lithium into the structure of semiconducting 2D MoS_2 leads to the formation of 2D lithium molybdenum disulfide (Li_xMoS_2, $0 < x \leq 1$) which has metallic

properties.[8] Therefore, the bilayer structures with both intercalated 2H and 1T crystal phases were calculated using the first principles density functional theory (DFT). Figure 2 shows the total density of states for bilayer 2H and 1T MoS_2 and their lithium intercalated cases. As expected, pristine 2H MoS_2 and 1T MoS_2 demonstrate semiconducting and metallic behavior, respectively.[17] Upon Li^+ ions intercalation, we observe that the semiconducting nature of 2H MoS_2 becomes metallic, while the metallic 1T MoS_2 remains metallic in agreement with experimental observations.[30, 31] The formation of 2D metallic Li_xMoS_2 can be experimentally confirmed by photoluminescence (PL) quenching of nanoflakes after Li^+ ions intercalation (Figure 3a), which evidence that transition of the nanoflakes from originally semiconducting to eventually metallic phase.[17, 29, 32] The PL properties can be reversibly controlled by intercalation/deintercalation of Li^+ ions that is discussed in Supporting Information Section S3.

To estimate how much lithium is intercalated into 2D MoS_2, calculations of the ratios of 2H to 1T Mo $3d_{5/2}$ peak areas from XPS are conducted. The result shows that the ratio at the applied voltage of –6 V is ~1.3, suggesting that the content *x* is in the range of 0.3–0.5.[33] For the applied voltages of –8 and –10 V, the ratio is approximately 0.8, corresponding to a value for *x* in the range of 0.5 to 0.8.[33]

The plasmonic properties of these intercalated 2D nanoflakes are revealed by investigating the optical absorption characteristics in the UV-Vis regions after the Li^+ ions intercalation. In order to estimate the locations of plasmon resonances, the theoretical absorption peaks are firstly obtained based on the calculated extinction coefficients (Equation (1)) using Mie-Gans theory as a function of the specific amount of the intercalated Li^+ ions[3, 15]

$$A\ \alpha\ \omega\varepsilon_m^{\frac{3}{2}}\sum_{\mathrm{j}}\frac{\left[\frac{1}{{p_\mathrm{j}}^2}\right]\varepsilon_2}{\left[\varepsilon_1+\frac{1-p_\mathrm{j}}{p_\mathrm{j}}\varepsilon_m\right]^2+{\varepsilon_2}^2} \qquad (1)$$

in which ω is the angular frequency of incident light; ε_m is the dielectric constant of the medium, ε_1 and ε_2 are the real and imaginary terms of the dielectric function, respectively, and p_j are the depolarization factors for the three axes A (length), B (thickness) and C (width) of the nanoflakes. The length and width are considered to be equal in the 2D system. The depolarization factors for a 2D material are defined as:[34]

$$\mathrm{P_B}=\frac{1}{g^2}\left[1-\left(\frac{1-g^2}{g^2}\right)^{\frac{1}{2}}\sin^{-1}g\right] \qquad (2)$$

$$\mathrm{P_A}=\mathrm{P_C}=\frac{1-\mathrm{P_B}}{2} \qquad (3)$$

where the g factor is:

$$g=\left(\frac{\mathrm{a}^2-\mathrm{b}^2}{\mathrm{a}^2}\right)^{1/2} \qquad (4)$$

The dielectric function is described by the Lorentz model:[34]

$$\varepsilon(\omega)=\varepsilon_1+\mathrm{i}\varepsilon_2=\varepsilon_b-\frac{{\omega_\mathrm{p}}^2}{\omega^2+\mathrm{i}\gamma\omega} \qquad (5)$$

in which ω_p is the bulk plasma frequency, ε_b is the polarization response from the core electrons (background permittivity), which is equal to 1 (the choice of this number is justified in Supporting Information Section S4) and γ is the damping coefficient of the resonance.

$$\omega_\mathrm{p}=\sqrt{\frac{Ne^2}{\varepsilon_0 m_e}} \qquad (6)$$

where the charge carrier density, N, can be calculated using Equation (7) and number of Li in the occupation site and volume of unit cell for 2H and 1T MoS_2 are listed in Supporting Information Tables S3 and S4. The calculated *N* is also listed.

$$Charge\ carrier\ density\ (N) = \left(\frac{Number\ of\ Li\ in\ the\ occupation\ site}{volume\ of\ unit\ cell}\right) \quad (7)$$

γ is the calculated using:

$$\gamma = \frac{1}{\tau} = \frac{n \times e^2}{\sigma m_e} \quad (8)$$

where ε_0 is the permittivity of free space, the effective mass of an electron is $m_e = m_o$, τ is the scattering time of an electron and the conductivity (σ) is estimated to be in the range of 10^2 – 10^3 Ω^{-1} cm^{-1} depending on the degree of Li^+ ion intercalation.[35]

It is observed that plasmonic absorption is largely dependent on the Li intercalation level as shown in Figure 4 (a). In this figure, the values for *x* are selected based on the theoretical calculations presented by Enyashin *et al*..[29] As *x* increases the wavelength of plasmon resonance absorption decreases from 714 to 263 nm, for both intercalated 2H (shown in the range of 0.125 to 0.5) and 1T phases (shown in the range of 0.25 to 1) of 2D nanoflakes, but at a slower pace when *x* exceeds 0.5. The ranges for *x* for each phase are selected based on the actual observed values.[36]

The theoretical calculations are compared with the experimental results, in which they are obtained using UV-vis spectroscopy. From Figure 3b, it is noticed that there is no obvious absorption peak in the UV-vis spectrum for Li^+ ion intercalated MoS_2 nanoflakes at the applied voltage of –4 V, which confirms Li^+ ions are not able to efficiently dope MoS_2.[9] At this level, it seems that the nanoflakes do not contain enough free electrons to produce plasmon. When the voltage is decreased to –6 V, several absorption peaks are observed. The

peak locations are in very good agreement with theoretical estimates of the peaks (Figure 4 (a)) that correspond to x = 0.625 (336 nm), 0.5 (371 nm), 0.375 (424 nm), 0.25 (509 nm) and 0.125 (714 nm). The peaks can be associated with the formation of both metallic intercalated 1T and 2H phases. It is suggested that 2H and 1T phases coexist at $x \approx 0.25$.[33] Interestingly, observing that two very distinct prominent peaks at 380 and 714 nm appear, it seems that the peaks are generated by individual flakes of dissimilar electronic structure: some acquire 1T phase and the rest still remain in 2H phase. Interestingly, when the applied voltage is decreased to −8 V the peak at 714 nm decreases in intensity, while all other peaks become more prominent. Interestingly, there is also no gradual shift of the 714 nm peak after increasing the intercalation intensity by applying smaller voltages. At this voltage, x gains a larger average value (above 0.5), which is also confirmed by XPS (Figure 1f). The increase in the intensity of peaks (excluding 714 nm peak) can be mostly due to the enhancement and dominance of the metallic intercalated 1T phase. At −10 V, the peak at 714 nm is completely vanished, which evidences that only 1T phase exist at such high intercalation intensities. The clear transformation of the plasmon resonance peaks as a result of 2H to 1T phase conversion is different to that of conventional semiconductors for which a gradual shift in the resonance plasmon peak is seen when the doping level changes.[3] Furthermore, a discussion on the plasmon resonance quality (Q) factor of the intercalated 2D MoS_2 can be found in Figure S4 and Supporting Information Section S8.

The plasmon resonance presence from the intercalated MoS_2 nanoflakes is also assessed by electron energy loss spectroscopy (EELS) as shown in Figure S5. Gaussian peak fitting technique is used for extracting the plasmon, core-loss transition and the interband transition modes. Figure S5a demonstrates the EELS patterns collected from the 2D MoS_2 nanoflakes before Li^+ intercalation for comparison. It is important to consider that residual electrolyte $LiClO_4$ can stay there even after the comprehensive washing of the surface of nanoflakes,

which can affect the measurement. The deconvoluted peak at 4.0 eV can be ascribed to the interband transition.[37] Prominent peaks at 8.2, 18.0 and 24.1 eV are also observed, which correspond to the plasmon modes induced by valence electrons in different composite outer atomic cells.[38] The peaks at 29.5 and 44.3 eV can be assigned to the core-loss transition.[39] After the Li^+ intercalation at −10 V, two new peaks appearing at 3.2 and 6.7 eV are attributed to the surface and bulk plasmon modes originated by the free electrons generated from the Li^+ ions intercalation, respectively. This can also be verified by the Mie-Gans theoretical calculations detailed in Equations (1) and (6), in which the calculated surface and bulk plasmon energies are found to be at ~ 3.3 and ~ 6.5 eV, respectively. Interestingly, the original peak located at 4 eV, which is ascribed to the interband transition energy loss, disappears, indicating the semiconductor to metal transition. This is consistent with the DFT results shown in Figure 2. It is also noticed that the plasmon peaks originally at 8.2 and 24.1 eV for pristine 2D MoS_2 exhibit shifts to high energies of 11.2 and 27.1 eV after the intercalation, probably due to the change of oxidation states of Mo in the intercalated compounds.[40] Such change also results in the appearance of two new peaks at ~35 and 52 eV, indicating the variation of the core-loss transition energies of the intercalated compound.[40] The same discussion for the plasmon resonance observed at ~700 nm was not possible due to the weak EELS features.

The strong dependence of plasmon resonance wavelength to the surrounding dielectric environment is another unique characteristic according to Equation (1). Only the stronger plasmon resonance obtained at −10 V is investigated to be consistent with the EELS measurements. By varying the type of the surrounding solvent, the plasmonic band of ultra-doped MoS_2 nanoflakes experiences a red-shift of ~9 nm as the refractive index of surrounding solvent is increased from ~1.33 (methanol) to ~1.52 (o-xylene), which is in good agreement with the trend of theoretical calculations (Figure 4 (b)). The existence of the

localized plasmon enhancement effect of the ultra-doped nanoflakes (obtained at the applied voltage of −10 V) is also demonstrated by surface plasmon mediated fluorescence microscopy (SPMFM) as presented in Figure 5a. The surface plasmon mediated fluorescence effect only observed when sufficient amount of semiconducting 2D MoS_2 for producing PL coexist with large amount of 2D metallic Li_xMoS_2 for the excitation of the surface plasmon.[41] According to XPS data presented in Section S10, the surface is still made of a small amount of none intercalated 2D MoS_2, while the bulk of the film is highly intercalated Li_xMoS_2. The non-intercalated surface content is not sufficient to produce any PL upon normal to the surface incident light. However, if the incident light angle is equal to or above a critical angle, surface plasmon is generated that couples a large amount of energy to this remaining small 2D MoS_2 content. The transferred energy from the plasmonic 2D flakes underneath significantly enhances the surface PL, making it detectable.

In order to demonstrate a practical application for the created 2D plasmonic Li_xMoS_2 nanoflakes, a BSA based optical biosensing system is constructed. The suspended Li_xMoS_2 nanoflakes at an applied voltage of –10 V are incubated in a BSA solution (concentration of 50 mg mL^{-1}); UV-vis absorption measurements before and after the incubation are presented in Figure 5b. The plasmon resonance peak of 2D Li_xMoS_2 nanoflakes experiences a red shift to 390 nm after the BSA incubation. Due to the Li^+ intercalation, free electrons are generated within Li_xMoS_2 nanoflakes. When the BSA is incubated onto Li_xMoS_2 nanoflakes, the negatively charged immobilized BSA repels the free charges,[42] leading to a decrease in the electron density near the surface of the nanoflakes and hence causing a red shift of the surface plasmon resonance peak.

In summary, we successfully demonstrated plasmon resonances of ultra-doped 2D MoS_2 nanoflakes in the visible and near UV regimes by the electrochemical intercalation/de-

intercalation of Li^+ ions into and out of 2D MoS_2 nanoflakes. The doping level was controlled by the electrochemical forces, allowing the emergence of the plasmon resonance peaks due to the formation of semi metallic states. The applied electrochemical voltages of less than –6 V facilitated the transition of semiconducting MoS_2 to metallic Li_xMoS_2, while voltages less than –8 V resulted in the transformation from intercalated 2H to 1T phase. The EELS and solvent effect were used for confirming the presence of plasmon resonances. The theoretical calculations of the plasmon resonances were in agreement with the measurements, which further confirmed that the plasmonic of ultra-doped 2D flakes was the possible reason for the observations. An application of the nanoflakes was demonstrated using a model BSA based biosensing process. The presented 2D flakes have a great potential for future plasmonic biosensing and optical systems.

Methods. *Synthesis of 2D MoS_2 nanoflakes.* One gram of MoS_2 powders (99% purity, Sigma Aldrich) is added to 0.5 mL of NMP (99% anhydrous, Sigma Aldrich) in a mortar and ground for 30 min. The mixture is placed in vacuum oven to dry overnight at room temperature, then is collected and re-dispersed into a 10 mL NMP solvent. The solution is probe-sonicated (Ultrasonic Processor GEX500) for 90 min at a power of 125 W and the supernatant containing 2D MoS_2 nanoflakes is collected after being centrifuged for 45 min at a speed of 4000 rpm.

Intercalation of Li^+ ions into the 2D MoS_2 nanoflakes. 100 µL of the MoS_2 supernatant is drop-casted onto a conductive FTO coated glass substrate with an exposed area of ~0.5 cm^2 at ~60 °C. An applied voltage of –4 to –10 V is introduced using a two-electrode configuration *via* a DC power supply where the cathode is connected to the drop-casted MoS_2 film and the anode is a platinum wire. The electrolyte is 0.1 M $LiClO_4$ (98% purity, Sigma Aldrich) in polypropylene carbonate (97% anhydrous, Sigma Aldrich).

Characterization of 2D MoS_2 and Li_xMoS_2 nanoflakes. The crystal structures are characterized using HRTEM (JEOL 2100F). The Raman spectra are obtained using Horiba TRIAX 320 spectrometer, fiber-coupled to an Olympus BX41 confocal microscope with 532 nm 90 μW excitation. XRD is conducted with Bruker D4 Endeavour wide-angle diffractometric with a (Cu K-alpha) 0.15418 nm X-ray source. XPS measurements (VG MicroLab VG-310F) are performed using Al non-monochromated X-rays (20 kV, 15 mA) with the hemispherical energy analyzer set at a pass energy of 20 eV for the peak scans. Single phase etching, with ion energy of 1 keV, was performed. The etching time was 60 s. The absorbance spectra of 2D nanoflakes are examined using a UV-Vis-NIR microspectrophotometer (CRAIC 20/30 PV). The PL intensities of 2D nanoflakes are measured using a Nikon epi-fluorescence microscope with a blue excitation light source covering the wavelengths of 400 to 500 nm. SPMFM imaging of 2D nanoflakes is carried out using a total internal reflection fluorescence microscope (Nikon Eclipse Ti) operated at the laser wavelength of 405 nm. In order to obtain the electron energy loss spectra, a high-angle annular dark field (HAADF)-STEM image of the region of interest is first acquired. Then, a small area map is acquired across the nanoflakes and the total number of data points is determined. The spectra are collected at every 2 nm interval. The zero loss peak (ZLP) of each spectrum is aligned using a digital micrograph (DM) and removed using the reflected tail model. To evaluate the biosensing capability of 2D MoS_2 nanoflakes, BSA solutions (Invitrogen) with concentration of 50 mg mL^{-1} is incubated with 100 μL of suspended Li_xMoS_2 solution for 0.5 h. The absorption spectra are measured afterwards.

Dielectric effect on the plasmon resonance. MoS_2 nanoflakes are intercalated at –10 V as described before. The electrolyte was removed and subsequently replaced with o-xylene, cyclohexane and methanol solutions. For each solvent, the nanoflakes are left for 5 mins to ensure adequate perfusion, following which UV-Vis measurements are taken from the flakes

and background were corrected.[43] The peak fitting algorithm using Gaussian models was used to determine the location and intensity of the plasmonic band.

Computational methods. The first principles DFT (Vienna *Ab Initio* Simulation Package)[44] for electronic structure calculations was used to demonstrate the transition from semiconducting 2H MoS_2 to metallic intercalated Li_xMoS_2. The generalized gradient approximation in the form of Perdew-Burke-Ernzerhof was employed to describe the exchange-correlation functional.[45] The projector augmented wave potentials are used to model the core and valence electronic interaction.[46] The electrons in $1s^2 2s^1$, $4p^6 5s^1 4d^5$, $2s^2 3p^4$ states are treated as valence electrons for Li, Mo and S, respectively. The kinetic energy cut-off of 600 eV and a 21×21×1 Γ-centered mesh for sampling the Brillouin zone of bilayer MoS_2 are used to ensure the variation in total energy is less than 1 meV/atom. Optimised lattice parameters are obtained by allowing cell vectors and ionic positions to fully relax until the Hellmann-Feynman forces are less than 0.01 eV/Å. For accurate density of states calculations we use a 45×45×1 Γ-centered mesh for sampling the Brillouin zone and 800 eV energy cut-off. In all cases, Grimme's DFT-D2 method is used to correctly describe interlayer van der Waals interactions.[47-49] In order to study the effect of Li^+ intercalation on the electronic structure of MoS_2, a 1x1 bilayer unit cell for both 2H and 1T MoS_2 polytypes are selected. Li atoms are sequentially introduced in the low-energy octahedral binding sites and the intercalated bilayer structure is again optimized.

AUTHOR INFORMATION

Corresponding Authors

***E-mail:** kourosh.kalantar@rmit.edu.au

***E-mail:** jianzhen.ou@rmit.edu.au

***E-mail:** yichaowang@gmail.com

Notes

The authors declare no competing financial interest.

ACKNOWLEDGEMENT

The authors acknowledge support from the Australian Research Council (ARC) through Discovery Project DP140100170. The authors would also like to acknowledge the facilities as well as scientific and technical assistance of the Australian Microscopy & Microanalysis Research Facility at the RMIT University Microscopy & Microanalysis Facility, and the Micro Nano Research Facility (MNRF) at RMIT University.

SUPPORTING INFORMATION

Lateral size and thickness distributions of 2D MoS_2 nanoflakes; Mean crystallite dimension of lithium intercalated 2D MoS_2 nanoflakes at different applied voltages; Active control of PL in 2D MoS_2 nanoflakes; Value for infinite frequency dielectric constant; Optical absorption measurement of lithium intercalated FTO substrate; Plasmon resonance quality factor for Li_xMoS_2; EELS spectra of 2D MoS_2 and 2D Li_xMoS_2; XPS pattern of elemental Mo at surface for not etched and etched films. This material is available free of charge *via* the Internet at http://pubs.acs.org.

REFERENCES

1. Barnes, W. L.; Dereux, A.; Ebbesen, T. W. *Nature* **2003,** *424*, 824-830.

2. Maier, S. A.; Atwater, H. A. *Appl. Phys. Lett.* **2005,** *98*, 011101.

3. Naik, G. V.; Shalaev, V. M.; Boltasseva, A. *Adv. Mater.* **2013,** *25*, 3264-3294.

4. West, P. R.; Ishii, S.; Naik, G. V.; Emani, N. K.; Shalaev, V. M.; Boltasseva, A. *Laser Photon. Rev.* **2010,** *4*, 795-808.

5. Hoffman, A. J.; Alekseyev, L.; Howard, S. S.; Franz, K. J.; Wasserman, D.; Podolskiy, V. A.; Narimanov, E. E.; Sivco, D. L.; Gmachl, C. *Nat. Mater.* **2007,** *6*, 946-950.

6. Scholz, A.; Stauber, T.; Schliemann, J. *Phys. Rev. B* **2013,** *88*, 035135.

7. Wang, Y.; Ni, Y. *Anal. Chem.* **2014,** *86*, 7463-7470.

8. Wang, Y.; Ou, J. Z.; Balendhran, S.; Chrimes, A. F.; Mortazavi, M.; Yao, D. D.; Field, M. R.; Latham, K.; Bansal, V.; Friend, J. R.; Zhuiykov, S.; Medhekar, N. V.; Strano, M. S.; Kalantar-zadeh, K. *ACS Nano* **2013,** *7*, 10083-10093.

9. Ou, J. Z.; Chrimes, A. F.; Wang, Y.; Tang, S. Y.; Strano, M. S.; Kalantar-zadeh, K. *Nano Lett.* **2014,** *14*, 857-863.

10. Ambrosi, A.; Sofer, Z.; Pumera, M. *Small* **2014**, **DOI:** 10.1002/smll.201400401.

11. Mak, K. F.; Lee, C.; Hone, J.; Shan, J.; Heinz, T. F. *Phys. Rev. Lett.* **2010,** *105*, 136805.

12. Radisavljevic, B.; Radenovic, A.; Brivio, J.; Giacometti, V.; Kis, A. *Nat. Nanotechnol.* **2011,** *6*, 147-150.

13. Lopez-Sanchez, O.; Lembke, D.; Kayci, M.; Radenovic, A.; Kis, A. *Nat. Nanotechnol.* **2013,** *8*, 497-501.

14. Yamamoto, M.; Einstein, T. L.; Fuhrer, M. S.; Cullen, W. G. *J. Phys. Chem. C* **2013,** *117*, 25643-25649.

15. Manthiram, K.; Alivisatos, A. P. *J. Am. Chem. Soc.* **2012,** *134*, 3995-3998.

16. Eda, G.; Fujita, T.; Yamaguchi, H.; Voiry, D.; Chen, M.; Chhowalla, M. *ACS Nano* **2012,** *6*, 7311-7317.

17. Eda, G.; Yamaguchi, H.; Voiry, D.; Fujita, T.; Chen, M.; Chhowalla, M. *Nano Lett.* **2011,** *11*, 5111-5116.

18. Chhowalla, M.; Shin, H. S.; Eda, G.; Li, L.-J.; Loh, K. P.; Zhang, H. *Nat Chem* **2013,** *5*, 263-275.

19. Yao, Y.; Tolentino, L.; Yang, Z.; Song, X.; Zhang, W.; Chen, Y.; Wong, C. P. *Adv. Funct. Mater.* **2013,** *23*, 3577-3583.

20. Coleman, J. N.; Lotya, M.; O'Neill, A.; Bergin, S. D.; King, P. J.; Khan, U.; Young, K.; Gaucher, A.; De, S.; Smith, R. J.; Shvets, I. V.; Arora, S. K.; Stanton, G.; Kim, H.-Y.; Lee, K.; Kim, G. T.; Duesberg, G. S.; Hallam, T.; Boland, J. J.; Wang, J. J.; Donegan, J. F.; Grunlan, J. C.; Moriarty, G.; Shmeliov, A.; Nicholls, R. J.; Perkins, J. M.; Grieveson, E. M.; Theuwissen, K.; McComb, D. W.; Nellist, P. D.; Nicolosi, V. *Science* **2011,** *331*, 568-571.

21. Spahr, M. E.; Novák, P.; Haas, O.; Nesper, R. *J. Power Sources* **1995,** *54*, 346-351.

22. Alsaif, M. M. Y. A.; Latham, K.; Field, M. R.; Yao, D. D.; Medehkar, N. V.; Beane, G. A.; Kaner, R. B.; Russo, S. P.; Ou, J. Z.; Kalantar-zadeh, K. *Adv. Mater.* **2014,** *26*, 3931-3937.

23. Balendhran, S.; Ou, J. Z.; Bhaskaran, M.; Sriram, S.; Ippolito, S.; Vasic, Z.; Kats, E.; Bhargava, S.; Zhuiykov, S.; Kalantar-zadeh, K. *Nanoscale* **2012,** *4*, 461-466.

24. Li, H.; Zhang, Q.; Yap, C. C. R.; Tay, B. K.; Edwin, T. H. T.; Olivier, A.; Baillargeat, D. *Adv. Funct. Mater.* **2012,** *22*, 1385-1390.

25. Ling, X.; Fang, W.; Lee, Y.-H.; Araujo, P. T.; Zhang, X.; Rodriguez-Nieva, J. F.; Lin, Y.; Zhang, J.; Kong, J.; Dresselhaus, M. S. *Nano Lett.* **2014,** *14*, 3033-3040.

26. Balendhran, S.; Walia, S.; Nili, H.; Ou, J. Z.; Zhuiykov, S.; Kaner, R. B.; Sriram, S.; Bhaskaran, M.; Kalantar-zadeh, K. *Adv. Funct. Mater.* **2013,** *23*, 3952-3970.

27. Liu, N.; Kim, P.; Kim, J. H.; Ye, J. H.; Kim, S.; Lee, C. J. *ACS Nano* **2014,** *8*, 6902-6910.

28. Wu, S.; Zeng, Z.; He, Q.; Wang, Z.; Wang, S. J.; Du, Y.; Yin, Z.; Sun, X.; Chen, W.; Zhang, H. *Small* **2012,** *8*, 2264-2270.

29. Enyashin, A. N.; Seifert, G. *Comput. Theor. Chem.* **2012,** *999*, 13-20.

30. Boker, T.; Severin, R.; Muller, A.; Janowitz, C.; Manzke, R.; Voss, D.; Kruger, P.; Mazur, A.; Pollmann, J. *Phys. Rev. B* **2001,** *64*, 235305.

31. Mattheiss, L. F. *Phys. Rev. B* **1973,** *8*, 3719-3740.

32. Li, B. L.; Chen, L. X.; Zou, H. L.; Lei, J. L.; Luo, H. Q.; Li, N. B. *Nanoscale* **2014,** *6*, 9831-9838.

33. Wang, H.; Lu, Z.; Xu, S.; Kong, D.; Cha, J. J.; Zheng, G.; Hsu, P. C.; Yan, K.; Bradshaw, D.; Prinz, F. B.; Cui, Y. *Proc. Natl Acad. Sci. USA* **2013,** *110*, 19701-19706.

34. Papavassiliou, G. C. *Prog. Solid State Chem.* **1979,** *12*, 185-271.

35. Julien, C. M. *Mater. Sci. Eng. R-Rep.* **2003,** *40*, 47-102.

36. Benavente, E.; Santa Ana, M. A.; Mendizábal, F.; González, G. *Coord. Chem. Rev.* **2002,** *224*, 87-109.

37. Hong, J.; Li, K.; Jin, C.; Zhang, X.; Zhang, Z.; Yuan, J. *ArXiv e-prints* **2014,** *1409*, 1409.

38. Kumar, A.; Ahluwalia, P. K. *Physica B* **2012,** *407*, 4627-4634.

39. Bell, M. G.; Liang, W. Y. *Adv. Phys.* **1976,** *25*, 53-86.

40. Schubert, W. K.; Wolf, E. L. *Phys. Rev. B* **1979,** *20*, 1855-1862.

41. Gómez, D. E.; Vernon, K. C.; Mulvaney, P.; Davis, T. J. *Nano Letters* **2009,** *10*, 274-278.

42. Balendhran, S.; Walia, S.; Alsaif, M.; Nguyen, E. P.; Ou, J. Z.; Zhuiykov, S.; Sriram, S.; Bhaskaran, M.; Kalantar-zadeh, K. *ACS Nano* **2013,** *7*, 9753-9760.

43. Cadusch, P. J.; Hlaing, M. M.; Wade, S. A.; McArthur, S. L.; Stoddart, P. R. *J. Raman Spectrosc.* **2013,** *44*, 1587-1595.

44. Kresse, G.; Furthmuller, J. *Phys. Rev. B* **1996,** *54*, 11169-11186.

45. Perdew, J. P.; Burke, K.; Ernzerhof, M. *Phys. Rev. Lett.* **1996,** *77*, 3865-3868.

46. Blochl, P. E. *Phys. Rev. B* **1994,** *50*, 17953-17979.

47. Kohn, W.; Meir, Y.; Makarov, D. E. *Phys. Rev. Lett.* **1998,** *80*, 4153-4156.

48. Grimme, S. *J. Comput. Chem.* **2006,** *27*, 1787-1799.

49. Bhattacharyya, S.; Singh, A. K. *Phys. Rev. B* **2012,** *86*, 075454.

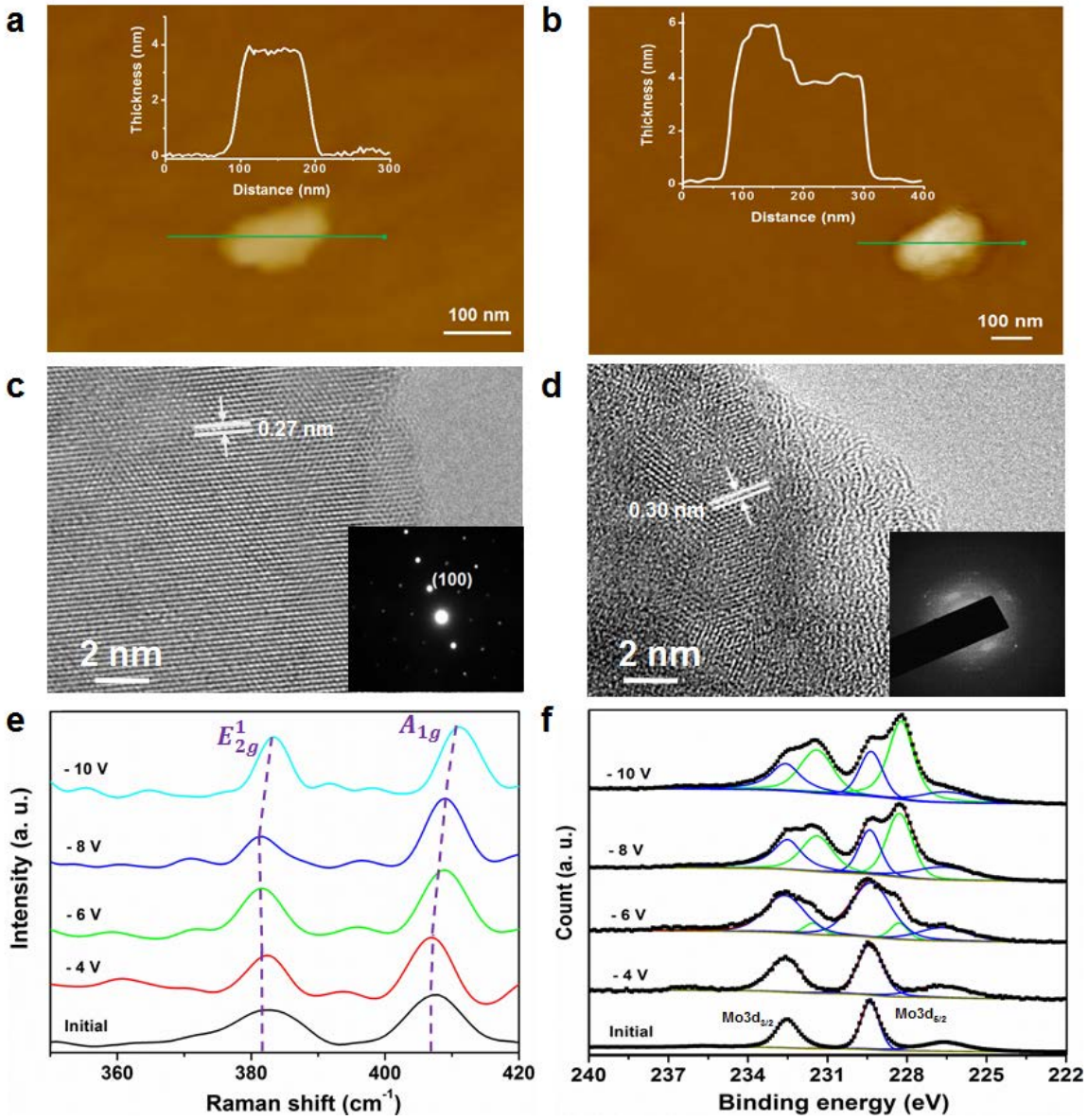

Figure 1. AFM and HRTEM images of flakes before and after the intercalation *via* a –10 V applied voltage are shown in **(a)** to **(d)**. Examples of the AFM images and profiles for a 2D MoS_2 nanoflake (a) and a 2D Li_xMoS_2 nanoflake **(b)**. **(c)** A HRTEM image of a pristine 2D MoS_2 nanoflake and its corresponding SAED pattern (inset). **(d)** A HRTEM image of an intercalated 2D nanoflake and its corresponding SAED pattern (inset). **(e)** Raman spectra of 2D MoS_2 and the spectra changes after Li^+ ion intercalation at different applied voltages. **(f)** XPS spectra of elemental Mo after Li^+ ion intercalation at different applied voltages (all XPS spectra are calibrated by a carbon 1s peak located at 284.50 eV). It is also noticed that a small peak appears at 236.0 eV, corresponding to Mo^{6+} $3d_{5/2}$, which is a common characteristic for Li^+ intercalated MoS_2, possibly due to the oxidation of a very small portion of MoS_2.

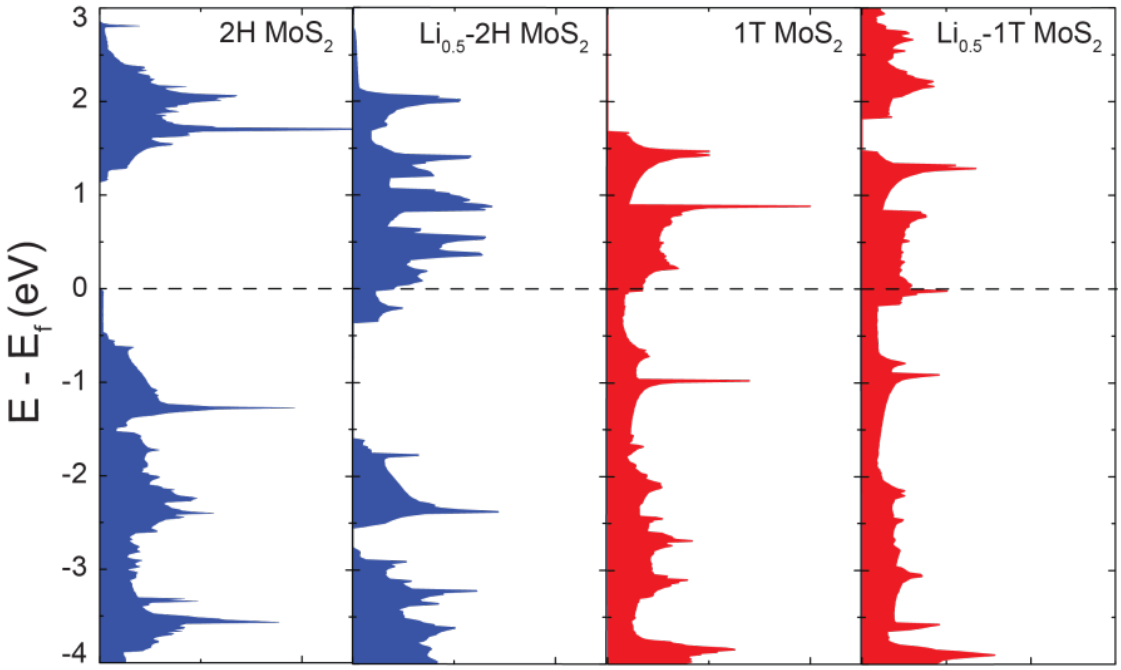

Figure 2. DFT calculations for a bilayer 2D MoS_2 nanoflake before and after Li^+ ion intercalation. Total density of states for bilayer 2H MoS_2 and 2H $Li_{0.5}MoS_2$ (Blue), and bilayer 1T MoS_2 and 1T $Li_{0.5}MoS_2$ (Red). The Fermi level is set to zero. It is noticed that the pristine 2H MoS_2 is a semiconductor with the bandgap of ~1.7 eV while pristine 1T MoS_2 is a quasi-metal. After the Li^+ ions intercalation, the conduction band of intercalated 2H MoS_2 are downshifted below the Fermi level and transformed into metallic, while intercalated 1T MoS_2 remains metallic. 0.5 of intercalated Li^+ is selected as an example.

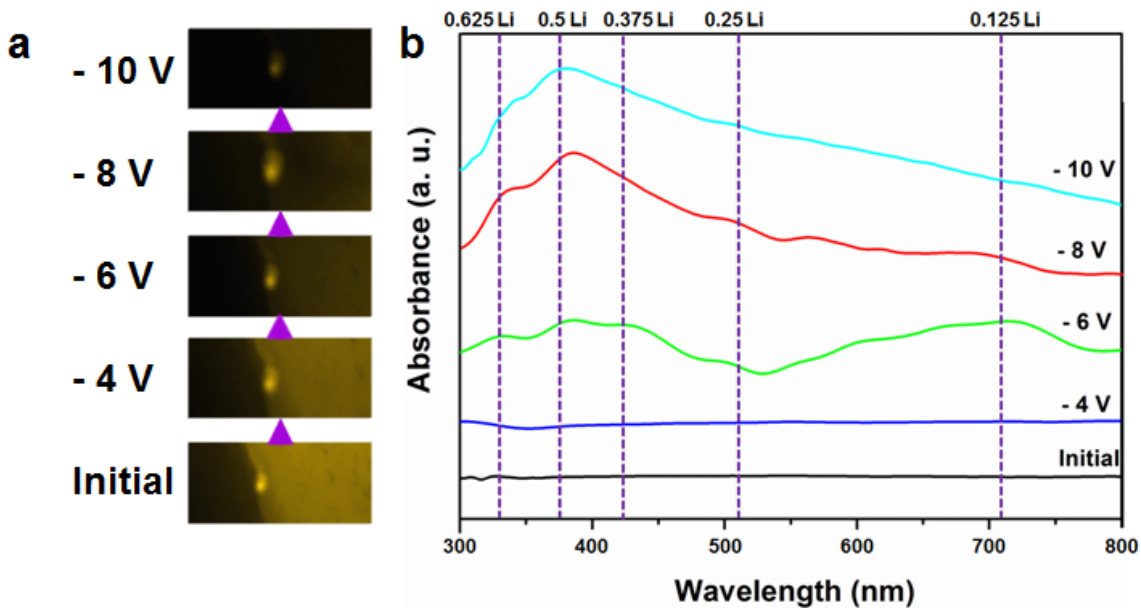

Figure 3. (a) PL images of films made of drop-casted 2D MoS_2 in initial and at the intercalating voltages of –4, –6, –8 and –10 V (at a broadband excitation light source covering wavelengths ranging from 400 to 500 nm.) The changes in PL of 2D nanoflakes at different applied voltages are presented. Yellow colored light is emitted from the 2D MoS_2 nanoflakes at the initial stage. When a voltage of –4 V is applied to the sample, the PL level is only slightly reduced. When the applied voltage is decreased from –6 to –10 V, PL intensity drops dramatically and there is a near total photo-quenching at the voltage of –10 V. (b) UV-Vis absorbance spectra of the 2D nanoflakes under different electrochemical forces, in which the pristine 2D MoS_2 is used as the differential reference. Main absorption peaks in the experimental are observed at 332, 380, 430, 498 and 714 nm. The wavelengths for theoretical estimates of plasmonic peaks as a function of intercalated Li^+ ions are listed along dot lines. An intercalated fluoride-doped tin oxide (FTO) peak is observed at 325 nm, showing a minimal interference (Figure S3 and Supporting Information Section S7).

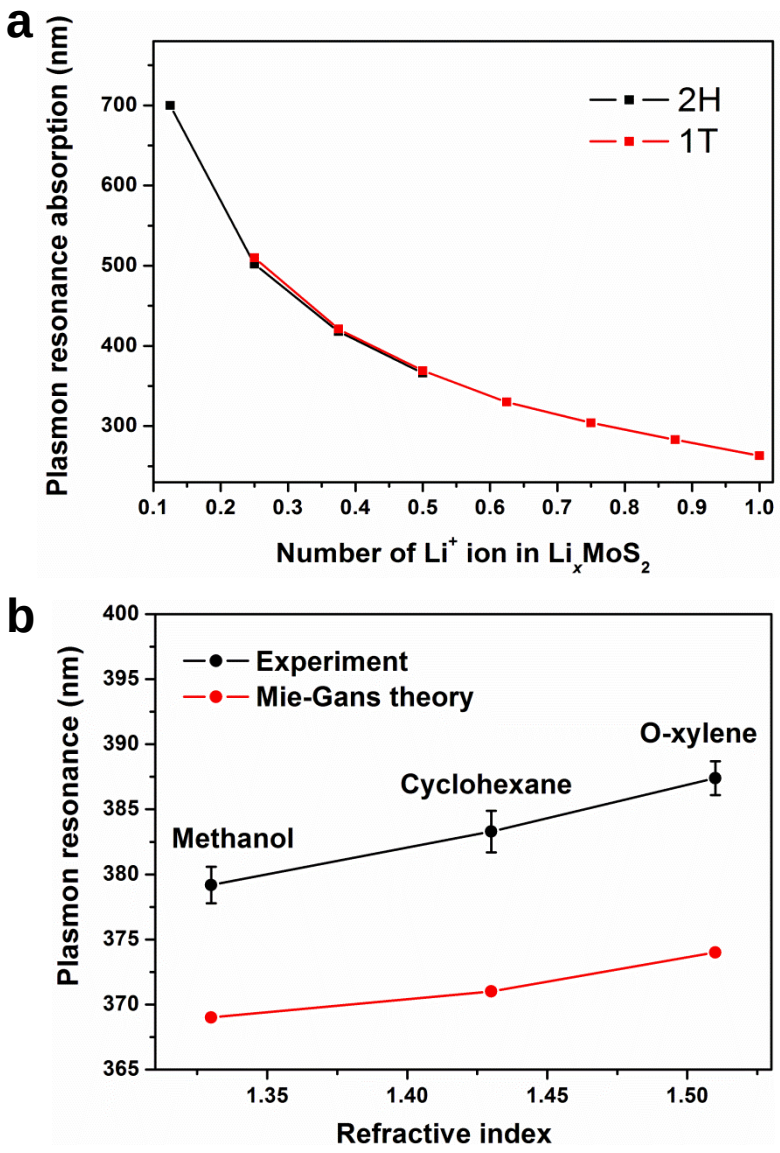

Figure 4. (a) Theoretical analysis for the correlation between the plasmon resonance peak positions and number of Li^+ ions in 2D MoS_2 nanoflakes for both intercalated 2H and 1T phases. (b) Experimental and theoretically calculated plasmon resonance peaks of ultra-doped MoS_2 in different dielectric environments.

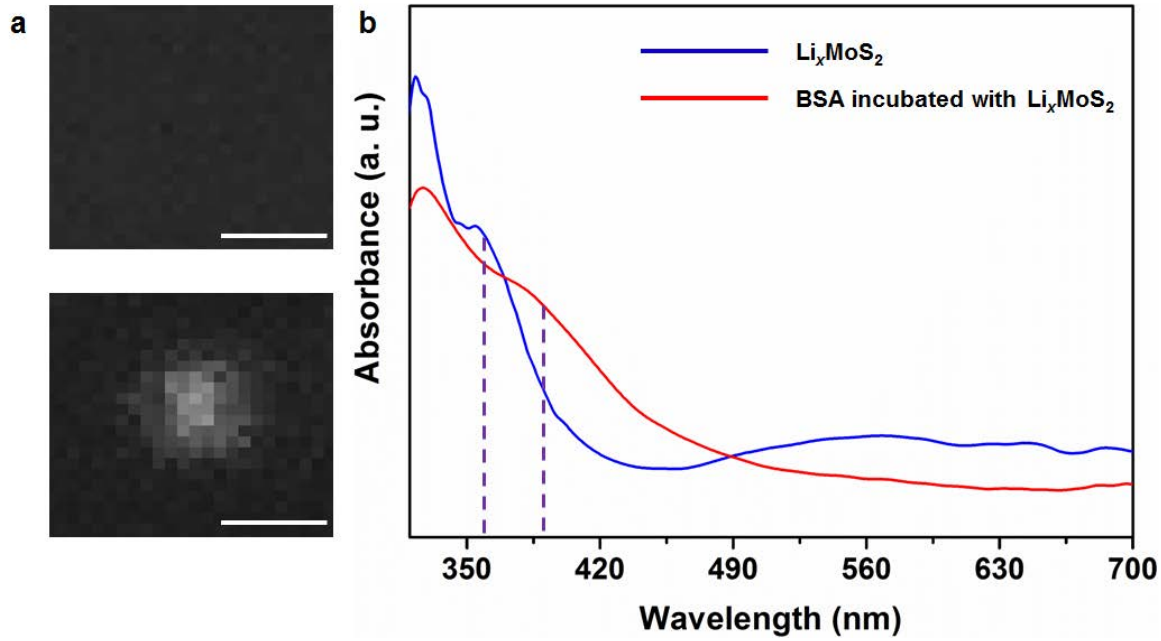

Figure 5. (a) Li^+ intercalated samples at the voltage of –10 V are exfoliated onto a cover glass substrate and SPMFM images are obtained. Based on Figure S6 and Supporting Information Section S10, it is found that the surfaces of these samples are restored to 2H MoS_2 while the bulk remains intercalated 1T metallic phase. When the 405 nm excitation laser source is used, no PL is seen, as most of the flakes are semi metallic with no band gap. After the source is tilted beyond the critical angle, light intensity of the flakes increases dramatically and observable bright spots are identified due to the surface plasmon generated by 1T intercalated flakes that greatly enhances the PL emitted from the restored 2H MoS_2. PL image of exfoliated nanoflakes (up) and SPMFM image of the same nanoflakes beyond the critical angle (down). Scale bar represents 1 µm. (b) Normalized absorption spectra of 2D MoS_2 nanoflakes after Li^+ ion intercalation both before (blue line) and after (red line) incubation with BSA at a concentration of 50 mg mL^{-1}. The absorption peak of ~325 nm, which is ascribed to the Li^+ intercalated FTO substrate (Figure S3 and Supporting Information Section S7), is observed due to the utilization of thinner sample for BSA sensing measurements. The initial plasmon peak located at ~360 nm is at a lower wavelength in comparison to that of seen in Figure 3b. This is also due to the utilization of a thinner sample, resulting in more Li^+ intercalation hence stronger doping effect under a similar applied electrochemical force.